Materials and Design 196 (2020) 109170

Contents lists available at ScienceDirect

Materials and Design

journal homepage: www.elsevier.com/locate/matdes

Processing maps based on polymerization modelling of thick methacrylic laminates

Sarah F. Gayot [a,b], Christian Bailly [b], Thomas Pardoen [a], Pierre Gérard [c], Frederik Van Loock [a,*]

[a] Institute of Mechanics, Materials & Civil Engineering, UCLouvain, Place Sainte-Barbe 2, 1348 Louvain-la-Neuve, Belgium
[b] Institute of Condensed Matter & Nanosciences, UCLouvain, Place Croix-du-Sud 2, 1348 Louvain-la-Neuve, Belgium
[c] Groupement de Recherche de Lacq, Arkema, Route Départementale 817, BP 34, 64170 Lacq, France

HIGHLIGHTS

- Thick composite laminates are produced via vacuum infusion and in-situ polymerization of a methyl methacrylate-based resin.
- Monomer boiling due to the self-accelerating polymerization reaction can lead to macro-sized voids in the laminate.
- A thermochemical model is developed to predict the maximum temperature within the laminate during in-situ polymerization.
- The predicted temperature profiles are in excellent agreement with those measured for different processing conditions.
- Processing maps reveal optimal heating conditions leading to short cycle times without thermally-induced cavitation.

GRAPHICAL ABSTRACT

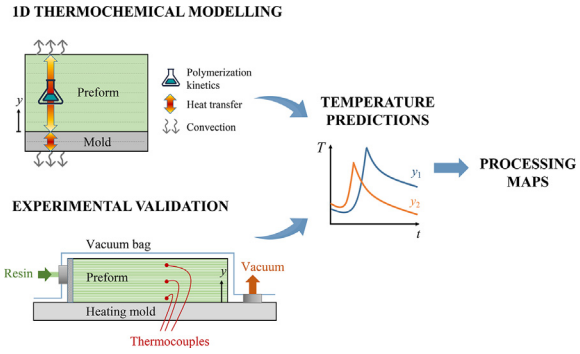

ARTICLE INFO

Article history:
Received 17 June 2020
Received in revised form 17 September 2020
Accepted 17 September 2020
Available online 22 September 2020

Keywords:
Polymer-matrix composite
Thermoplastic resin
Methyl methacrylate
Polymerization kinetics
Process monitoring
Thermochemical model

ABSTRACT

Control of the in-situ polymerization of thick methacrylic laminates is essential to minimize cavitation due to monomer boiling. To this end, a computationally efficient thermochemical model is developed to predict the temperature and degree of monomer conversion during polymerization of a methyl methacrylate (MMA)-based resin in a fibrous preform. The model couples the self-accelerating exothermic free-radical bulk polymerization of MMA (gel effect) with the heat transfer within the preform and to the environment. The predicted temperature profiles are in excellent agreement with experimental data measured during a series of in-situ polymerization tests with different heating conditions and preform thicknesses. Processing diagrams are constructed to reveal the regimes of interest for the production of thick fiber-reinforced methacrylic composites without voids induced by monomer boiling.

* Corresponding author.
E-mail addresses: sarah.gayot@uclouvain.be (S.F. Gayot), christian.bailly@uclouvain.be (C. Bailly), thomas.pardoen@uclouvain.be (T. Pardoen), pierre.gerard@arkema.com (P. Gérard), frederik.vanloock@uclouvain.be (F. Van Loock).

https://doi.org/10.1016/j.matdes.2020.109170

1. Introduction

The recyclability of lightweight materials of high specific strength and stiffness is an ongoing challenge in the composite manufacturing industry. This challenge is driving the transition from thermoset to recyclable thermoplastic matrices for fiber-reinforced polymer composites [1,2]. Dedicated thermoplastic resin formulations have been developed to ensure compatibility with existing liquid composite molding (LCM) manufacturing techniques. For instance, a range of methyl methacrylate (MMA)-based resins has been designed for the production of thermoplastic fiber-reinforced polymer composites via resin transfer molding or vacuum infusion [3–6]. During composite manufacturing via LCM, the monomer-based resin is infused through a preform, consisting of layers of glass or carbon fiber mats, before undergoing in-situ polymerization.

Composites produced by LCM techniques contain defects such as micro- and macro-sized voids. Porosity may have a significant and unpredictable impact on the mechanical behavior [7–11]. Voids nucleate and grow during the manufacturing process of epoxy-based composites due to a number of phenomena including incomplete resin degassing, air entrapment during mold filling, volatilization of resin components (or polymerization by-products) during in-situ curing, and/or matrix shrinkage upon curing and cooling [12–16]. Several process control strategies have been developed to reduce void nucleation and growth during LCM with epoxy resin [3,13,17–19].

The main source of cavitation during the manufacturing of MMA-based composites is through monomer boiling during in-situ polymerization [3,20,21]. As discussed by Murray et al. [1], a practical challenge arises when producing thick laminates (in the order of 1 cm and above). The free-radical polymerization kinetics of MMA exhibits a gel effect (known as Trommsdorff effect [22]): when the degree of monomer conversion exceeds a critical value, the exothermic reaction self-accelerates and the temperature increases. Voids nucleate and grow within the polymerizing matrix when the boiling temperature of the residual monomer is locally exceeded [20,21].

An external heat source is often used to reduce the polymerization time [23]. The external heating program can be adapted in order to control the maximum temperature within the preform and, therefore, void nucleation due to monomer boiling. The compromise between a short cycle time and the absence of porosity can be found via a trial-and-error approach, as is common practice in the industry. Alternatively, a thermochemical model, informed by in-situ process monitoring data, can guide this process design exercise by predicting the (maximum) temperature within the matrix as a function of processing parameters such as preform thickness and external heating rate. Such a model needs to account for (1) heat transfer within the molded preform and to the environment and (2) the release of heat due to the auto-accelerating exothermic reaction of MMA.

A large number of studies focus on the auto-accelerating nature of the polymerization of MMA. Trommsdorff [22] and Norrish and Smith [24] related the gel effect to a decrease of the coefficient quantifying the rate of radical termination k_t. The decrease of k_t occurs at a critical value of monomer conversion χ at which the diffusivity of the polymer radicals is significantly reduced. Analytical frameworks have been developed to predict the dependence of k_t upon χ, often based on the concept of free volume, see, for example, the work of Hamielec [25–27] and of Achilias [28–30]. Empirical models relating the sensitivity of k_t to χ also exist [31–34].

Many numerical thermochemical models have been developed to predict the curing temperature and the degree of monomer conversion during vacuum infusion of fiber-reinforced *thermoset* composites. Most of these make use of the approach of Loos and Springer [35] who constructed an experimentally validated one-dimensional (1D) framework coupling a heat equation with the curing kinetics of an epoxy matrix. Curing tests were conducted on relatively thick (up to 1.5 cm) carbon prepreg lay-ups in an autoclave and good agreement between the predicted and measured temperature profiles was observed. While many similar one- to three-dimensional models have been reported for the curing of thermoset composites [36–42], only a limited number of them are adapted to the polymerization of *thermoplastic* composites [21,43,44]. Borzacchiello et al. [43] and Suzuki et al. [21] have constructed 1D models to study the polymerization of methacrylate-based resins in composites. Borzacchiello et al. [43] combined the heat equation with a calibrated empirical model for the polymerization kinetics, and gave predictions for the temperature profiles measured during the polymerization of a methacrylic dental cement. Suzuki et al. [21] also solved the heat equation to predict the temperature and degree of monomer conversion during the in-situ polymerization of an MMA-infused glass fabric preform of thickness ranging from 10 cm to 50 cm. Suzuki and co-workers considered a preform sandwiched between two glass plates at constant temperature ($\approx$ 20 °C) and assumed the preform to be equivalent to a homogeneous slab of variable thickness. To reduce the computational cost, Suzuki et al. assumed the value of the termination coefficient k_t to be independent of temperature and of monomer conversion. Hence, their model does not account for the gel effect, and the predicted profiles are of qualitative nature.

The objective of this study is twofold. The first goal is to develop a thermochemical model for the in-situ polymerization of MMA in fiber-reinforced composites, which takes the auto-accelerating polymerization kinetics of MMA into account while being computationally efficient. Computationally efficient means that a parametric study can be performed at a reasonable computational cost (e.g. a few hours on a standard personal computer). The second goal is to apply the model to predict the temperature and the degree of monomer conversion across the thickness of an MMA-infused glass fiber layup as a function of key processing variables such as preform thickness and external heating rate. This allows the construction of processing diagrams based on the maximum temperature attained in the composite, which dictates the occurrence of monomer boiling (and thermally-induced cavitation).

2. Materials and experimental methods

2.1. Materials

Composite preforms were made from quasi-unidirectional non-crimp glass fabric plies (Chomarat, France) with an areal weight of 1.03 kg m^{-2} (85% warp and 15% weft). The resin comprised an infusion-grade monomer formula (Elium® 191OSA of Arkema, France) and a ketone peroxide thermal initiator (Luperox® K10 of Arkema, France). The Elium® 191OSA mixture contains MMA monomers with 20 to 30 wt% acrylic copolymer chains, which serve as a viscosifying agent. The consumables for bagging and infusion were obtained from Diatex SAS (France). The temperature within the preforms was measured during the infusion experiments using J-type thermocouples (TC S.A., France).

2.2. Composite manufacturing

Composite plates were manufactured via vacuum-assisted infusion using the setup illustrated in Fig. 1. Preforms were produced by laying

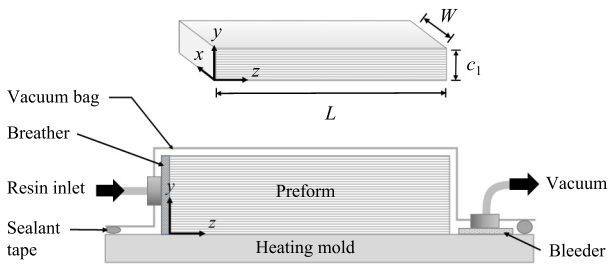

Fig. 1. Experimental setup for the vacuum infusion of laminates of variable thickness c_1 ($L = 60$ cm, $W = 40$ cm).

up glass fabric plies onto a heating mold. Three sets of manufacturing conditions, corresponding to plates A, B, and C, were explored. These conditions differ in preform thickness and heating mold set temperature as detailed in Table 1. The preforms consisted of 90 fabric plies for conditions A and B, and of 60 plies for condition C. Thermocouples were placed in the middle of the preform (at $x = W/2$, $z = L/2$, see Fig. 1) at three locations along the y-axis, see Table 1. Note that an additional test for conditions A and B was conducted. The measured temperature profiles at the top of the plate during the nominal and repeat tests for conditions A and B were close to identical. Each fiber stack was sealed with a vacuum bag and prepared for resin infusion. The resin mix was made with three parts initiator per hundred parts resin, mechanically stirred for 5 min, and then degassed for 1 min at a pressure close to 100 mbar. Infusion tests were conducted at a pressure close to 100 mbar at room temperature; the resin flows in the direction of the z-axis (i.e. aligned with the fiber tows). For all test conditions, the resin front reached the section instrumented with thermocouples (at $z = L/2$) when the process time t was close to 5 min (where $t = 0$ corresponds to the start of the infusion process). The resin inlet and vacuum outlet were clamped shut at the end of the infusion process. Then, for conditions B and C, the infused preform was heated via the heating mold from room temperature to a set temperature T_p equal to 50 °C (with a controlled heating rate close to 0.5 °C min^{-1}), see Fig. 2. The mold set temperature was maintained for 30 min, before the external heating was ceased. The polymerization of plate A occurred without any external heating. Upon completion of the polymerization reaction, at process time $t \gg t_3$ (see Fig. 2), the plate was left to cool down to room temperature and the composite was removed from the mold. Final fiber volume fractions were close to 0.5.

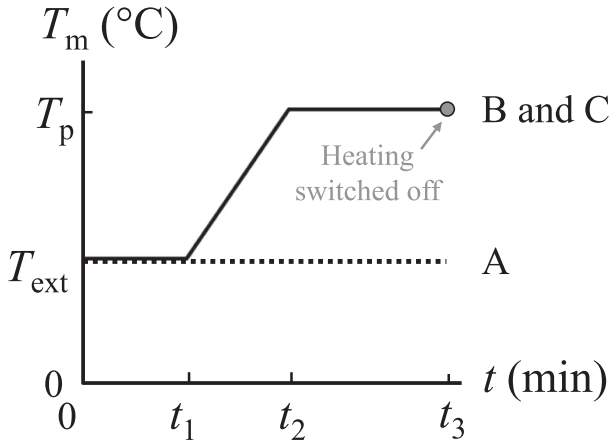

Fig. 2. Heating mold temperature T_m versus process time t for test conditions A, B and C, where T_{ext} denotes the ambient temperature, T_p (= 50 °C) the mold set temperature, t_1 (≈ 25 min) the end of the infusion stage, t_2 (≈ 75 min) the end of the heating ramp, and t_3 (≈ 105 min) the end of the temperature plateau at $T_m = T_p$.

2.3. Composite characterization

Cuboids of dimensions (10×13×10 mm^3) were machined from composite plates A and B using a water-cooled disk-milling cutter, according to the sectioning diagram shown in Fig. 3. A surface perpendicular to the fiber tow orientation was polished using resin-bonded diamond discs (successive grain size of P1200 and P4000) and an alumina suspension (de-agglomerated 0.05 μm alumina suspension of Allied, USA) for the finishing step. Micrographs of the polished surfaces were taken with an optical microscope (AX70 Provis, Olympus, Japan). The porosity Φ of the samples was measured by analyzing micrographs with the ImageJ [45] software. A computed tomography (CT) machine was used to confirm the accuracy of these measurements, see section II of the Supplementary Information.

3. Thermochemical model

3.1. Theory

A one-dimensional thermochemical model is developed to predict the temperature T, the concentration of monomer M and the degree of monomer conversion χ as a function of time t across the preform thickness. We assume the simulation time and the polymerization reaction to start when the resin front is at the simulation section of interest ($t = t_s$). In this work, predictions will be given at the laminate's half-length (at $z = L/2$) where the thermocouples are placed during the infusion tests. As detailed in section 2.2, $t_s = 300$ s. The infused composite preform is idealized as a slab of homogeneous material with a uniform thermal diffusivity α_1. It is recognized that the thermal diffusivity in the composite is of a heterogeneous nature and that the assumption of a uniform and

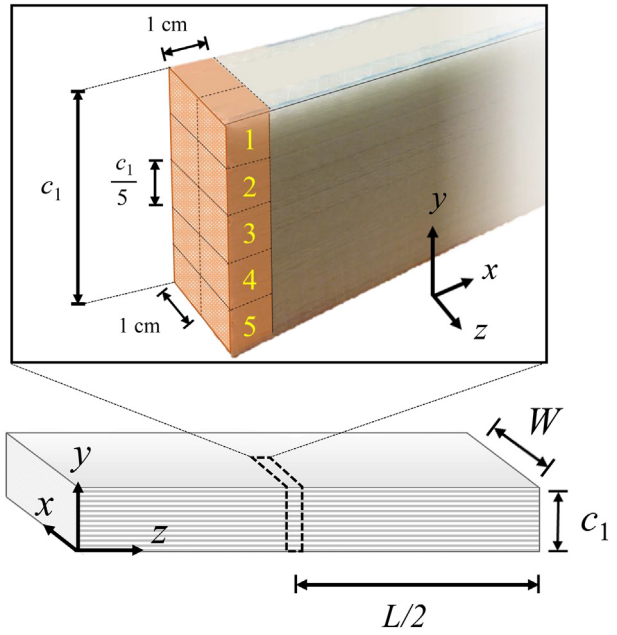

Fig. 3. Sectioning diagram for the characterization of plates A and B (L = 60 cm, W = 40 cm, c_1 = 73 mm).

Table 1
Summary of the processing conditions for tests A, B and C.

Experimental condition	A	B	C
Ambient temperature	$T_{ext} \approx 17$ °C	$T_{ext} \approx 25$ °C	$T_{ext} \approx 21$ °C
Laminate structure	90 plies, $(AB)_{45}/(BA)_{45,}$ symmetrical		60 plies, $(AB)_{30}/(BA)_{30,}$ symmetrical
Final part thickness	$c_1 = 73$ mm		$c_1 = 49$ mm
Location of thermocouples	Bottom: ply 5/90 ($y \approx 0.06c_1$)		Bottom: ply 5/60 ($y \approx 0.08c_1$)
	Middle: ply 45/90 ($y = 0.50c_1$)		Middle: ply 30/60 ($y = 0.50c_1$)
	Top: ply 85/90 ($y \approx 0.94c_1$)		Top: ply 55/60 ($y \approx 0.92c_1$)

time-independent value for the diffusivity, based on a rule of mixture, has a limited range of validity at the microscale. An extension of the model could include a time- and space-dependent thermal diffusivity. However, this extension is considered to lie beyond the scope of the present study. The values of T, M and χ are assumed to be independent of the transverse x and z coordinates, see Fig. 1 (i.e. edge effects are neglected close to the preform surfaces at the planes $x = 0, x = W, z = 0$, and $z = L$). The dependence of T upon position coordinate y and time t is calculated by solving the following heat equation:

$$\frac{dT}{dt} = \alpha_1 \frac{d^2T}{dy^2} - \frac{\Delta H}{C_p M_w^0} \frac{dM}{M_0 dt}. \quad (1)$$

The heat source term on the right-hand side of Eq. (1) accounts for the exothermic nature of the free-radical bulk polymerization reaction [21,35,43,44], where C_p is the specific heat capacity of the composite, ΔH is the enthalpy of polymerization, M_w^0 is the molecular weight of MMA, M_0 is the initial molar concentration of MMA in the preform, and dM/dt is the rate of change of monomer concentration. Both C_p and dM/dt are a function of y and t as detailed below. The value of C_p is based on the temperature-dependent specific heat capacity of the MMA monomer $C_{p,m}$, of the poly(methyl methacrylate) (PMMA) polymer $C_{p,p}$, and of the fiber $C_{p,f}$ via a rule of mixtures

$$C_p = (1-w_f)\underbrace{((1-\chi)C_{p,m} + \chi C_{p,p})}_{C_p \text{of resin matrix}} + w_f C_{p,f}, \quad (2)$$

where w_f is the mass fraction of the glass fibers.

Next, the value of dM/dt is calculated based on five coupled kinetic equations governing the polymerization of MMA. These kinetic equations are summarized in Table 2; the dependence of the kinetic constants upon T and χ is detailed in section I.A of the Supplementary Information. Several assumptions can be made to reduce the computing time. First, the long-chain hypothesis is invoked: polymer chains consist of a large number of monomer units (and this is experimentally validated for our system [46]), therefore the rate of propagation is much higher than the initiation rate r_i and the chain transfer rate $r_{tr,x}$. Flory's hypothesis is also used, i.e. the chemical reactivity of all propagating radicals is assumed to be equal. In addition, we apply the quasi-steady state approximation (QSSA) for the initiating and propagating radicals [47]. The QSSA is essential to reduce the computational cost of the model. This assumption is generally accepted to be valid for a free-radical polymerization without diffusional limitations [47]. However, the significant reduction of the termination constant k_t at the end of the polymerization reaction due to the gel effect may invalidate the use of the QSSA. This issue is discussed in detail in section I.B of the Supplementary Information. The conclusion of the analysis is that the QSSA for the MMA material system of interest remains valid up to a critical value of monomer conversion ranging from $\chi = 0.85$ to $\chi = 0.90$.

Table 2
Overview of the free-radical polymerization mechanism (M = MMA monomer, I = initiator, R_n• = macroradical with n monomer units, R• = all macroradicals, P = dead polymer, X = transfer agent, i.e. M, P, I or other molecule, f = initiator efficiency, C_x = transfer constant for chain transfer to transfer agent X).

Step	Equation	Kinetic coefficient	Reaction rate equation
Initiator decomposition	$I_2 \rightarrow 2\,I^\bullet$	k_d	$r_d = 2fk_d[I_2]$
Initiation	$I^\bullet + M \rightarrow IM^\bullet$	k_i	$r_i = k_i[I^\bullet][M]$
Propagation	$R_n^\bullet + M \rightarrow R_{n+1}^\bullet$	k_p	$r_p = k_p[R^\bullet][M]$
Termination by recombination	$R_n^\bullet + R_m^\bullet \rightarrow P_{n+m+2}$	k_t	$r_t = k_t[R^\bullet]^2$
disproportionation	$R_n^\bullet + R_m^\bullet \rightarrow P_{n+1} + P_{m+1}$		
Chain transfer	$R_n^\bullet + X \rightarrow P_n + X^\bullet$	$k_{tr,X}$	$r_{tr,X} = C_X k_p[R^\bullet][X]$

Consequently, the effect of the QSSA on the predicted time-temperature profiles up to, and including, the peak temperature due to the thermal excursion is considered to be small. Finally, only chain transfer reactions from the propagating radicals to the monomer and initiator molecules are considered. The rate of change of monomer concentration dM/dt then reads

$$\frac{dM}{dt} = -k_p M\sqrt{\frac{r_i}{k_t}} = -k_p M\sqrt{\frac{2fk_d I}{k_t}}, \quad (3)$$

where k_p, k_t and k_d are the rate coefficients of the radical propagation, radical termination and initiator decomposition steps, respectively, I is the initiator concentration and f is the efficiency factor of the initiator (equal to the fraction of initiating radicals that lead to the formation of polymer chains). In the case of MMA, polymerization is subject to various diffusional limitations: the values of k_t, k_p and f decrease with increasing conversion χ. The associated phenomena are known as the gel effect (as discussed above), the glass effect, and the cage effect, respectively [47]. The glass effect is related to a decrease in the mobility of monomer molecules (hence a decrease in k_p) as χ increases. The cage effect is related to a reduction of the mobility of newly-formed initiating radicals with increasing χ.

The free volume-based analytical model of Achilias et al. [29,30] is used to calculate the dependence of k_p, k_t, and f upon monomer conversion χ via the free volume V_f. The free volume of a polymer-solvent system is idealized as the ratio of the volume which is not occupied by the polymer chains or the solvent molecules to the total volume of the polymer-solvent system [48,49]. The equations for the dependence of k_p, k_t, and f upon T and χ are given in section I.A of the Supplementary Information. The modification of Achilias's theory [29,30] is a correction of the macroradicals diffusion constant in the entangled regime in order to account for the *effective* entanglement density. The values of the kinetic and physical parameters of the theory above are summarized in Tables 3 and 4.

3.2. Numerical implementation of the model

The thickness c_1 of the preform is discretized into N_y intervals Δy ($= c_1/N_y$, see Fig. 4). Likewise, the simulation time, which starts when the process time t is equal to t_s, is discretized into N_t time increments Δt ($= t_{tot}/N_t$), where t_{tot} is the total reaction time. In this study, we take $\Delta y = 1$ mm, $t_{tot} = 6 \times 10^4$ s and $\Delta t = 7$ s. Note that the selected value of t_{tot} includes the polymerization time of the resin and the cooling time of the plate.

Convective boundary conditions are considered at the top surface of the preform (i.e. at $y = c_1$, see Fig. 4):

$$\left(\frac{dT}{dy}\right)_{y=c_1} = \frac{h_1}{\lambda_1}(T_{y=c_1} - T_{ext}), \quad (4)$$

where h_1 is the convective heat transfer coefficient for the preform-air interface, λ_1 is the thermal conductivity of the polymer-based vacuum bag material, and T_{ext} is the ambient temperature outside the bag. A more sophisticated boundary condition is applied at the bottom and accounts for the transfer of heat from the preform to the infusion mold via conduction as follows. The mold consists of a homogeneous plate of thickness c_2 made of glass fiber reinforced polymer with a thermal diffusivity α_2, and covered with a polymeric heating film of thickness close to 0.1 mm. Therefore, the spatial mesh extends from $y = 0$ to $y = -c_2$ with nodes equally spaced by Δy, see Fig. 4. The temperature T on the nodes of the extended mesh is calculated as a function of time by solving the heat equation:

$$\frac{dT}{dt} = \alpha_2 \frac{d^2T}{dy^2}. \quad (5)$$

Table 3
Kinetic parameters and material properties for the infusion of a glass fiber preform with MMA.

Parameter	Symbol	Value	Unit	Reference
Weight fraction of glass fibers	w_f	≈ 0.73		this work
Preform diffusivity	α_1	2.4×10^{-7}	$m^2\ s^{-1}$	[50]
Mold diffusivity	α_2	3×10^{-7}	$m^2\ s^{-1}$	[50]
Thermal conductivity of vacuum bag	λ_1	0.2	$W\ m^{-1}\ K^{-1}$	[50]
Thermal conductivity of mold	λ_2	0.4	$W\ m^{-1}\ K^{-1}$	[50]
Thermal expansion coefficient of MMA	β_m	1.2×10^{-3}	K^{-1}	[51]
Thermal expansion coefficient of PMMA	β_p	2.1×10^{-4}	K^{-1}	[52]
Specific heat capacity of MMA	$C_{p,m}$	$114.1 + 6.83\ T$	$J\ kg^{-1}\ K^{-1}$	[53]
Specific heat capacity of PMMA	$C_{p,p}$	$-14.45 + 4.65\ T$	$J\ kg^{-1}\ K^{-1}$	[54]
Specific heat capacity of glass fiber	$C_{p,f}$	$442.1 + 1.24\ T$	$J\ kg^{-1}\ K^{-1}$	[55]
Specific volume of MMA	v_m	1.06×10^{-3}	$m^3\ kg^{-1}$	
Specific volume of PMMA	v_p	8.55×10^{-4}	$m^3\ kg^{-1}$	[54]
Glass transition of MMA	$T_{g,m}$	-126	°C	[56]
Glass transition of PMMA	$T_{g,p}$	114	°C	[56]
Free volume of MMA at glass transition temperature	$V_{g,m}$	0.025		[30]
Free volume of PMMA at glass transition temperature	$V_{g,p}$	0.025		[30]
Pre-exponential factor of the MMA diffusion coefficient	D_m^0	3.0×10^{-8}	$m^2\ s^{-1}$	[34]
Interaction radius of propagation	R_p	2.93×10^{-10}	m	[30,34,57]
Average entanglement spacing in PMMA	j_c	70		[54]
End-to-end distance per square root of number of monomer units in chain	δ	6.9×10^{-10}	m	[57]
Molecular weight of MMA	M_w^0	100.12	$g\ mol^{-1}$	[58]
Molecular weight between entanglements of PMMA	M_e	7000	$g\ mol^{-1}$	[54]
Initial monomer concentration of MMA	M_0	3700	$mol\ m^{-3}$	Not applicable
Initial initiator concentration	I	14	$mol\ m^{-3}$	Not applicable
Polymerization enthalpy of MMA	ΔH	57.8	$kJ\ mol^{-1}$	[54]
Pre-exponential factor for propagation	A_p	2.67×10^3	$m^3\ mol^{-1}\ s^{-1}$	[59]
Activation energy for propagation	E_p	22.36	$kJ\ mol^{-1}$	[59]
Pre-exponential factor for the termination rate coefficient	A_t	1.984×10^5	$m^3\ mol^{-1}\ s^{-1}$	[60]
Activation energy for termination	E_t	5.89	$kJ\ mol^{-1}$	[60]
Pre-exponential factor for initiator decomposition rate	A_d	4.017×10^5	s^{-1}	[61]
Monomer transfer coefficient	C_m	5×10^{-5}		[54]
Initiator transfer coefficient	C_i	6×10^{-2}		[54][a]

[a] Assumed to be equal to the value of C_i for dibenzoyl peroxide.

A convective boundary condition is considered at the bottom of the mold (i.e. at $y = -c_2$):

$$\left(\frac{dT}{dy}\right)_{y=-c_2} = \frac{h_2}{\lambda_2}\left(T_{y=-c_2} - T_{ext}\right), \tag{6}$$

where h_2 is the convective heat transfer coefficient for the mold/air interface and λ_2 is the thermal conductivity of the mold material. Note that, for processing conditions B and C, we impose the time-dependent temperature profile presented in Fig. 2 at node $y = -\Delta y$ to account for controlled external heating via the heating film.

The MATLAB computing environment is used for the implementation of the 1D thermochemical model detailed in section 3. The set of coupled equations is solved with the semi-implicit Crank-Nicolson finite difference method. The computing times for all predictions given in this article do not exceed 60 s on a standard personal computer (equipped with an Intel® CoreTM i7-4600U 2.10GHz processor and with 16 Gb of RAM).

4. Results and discussion

4.1. Infusion test results

Optical micrographs of samples extracted from plates A and B are shown in Fig. 5. The measured void content is sensitive to the heating program: the porosity of plate A is close to zero across the entire thickness, while the measured porosity in plate B increases from the bottom ($\Phi \approx 0$) to the top ($\Phi \approx 0.1$) of the plate. The measured temperature T_t at three locations along the thickness of plates A, B and C is plotted as a function of process time t in Fig. 6. A peak is observed on all time-temperature profiles; this is a signature of the gel effect. The measured temperature profiles are found to be sensitive to the measurement location along the y-axis of the preform: the maximum temperature increases from the bottom to the top of plates A and B, whereas the width of the peak decreases, see Fig. 6a. The peak temperature T_{max} on the measured profile of plate B is almost 20 °C higher than the peak temperature on the corresponding profile of plate A.

Table 4
Fitting parameters of the thermochemical model, including their selected values and imposed range of acceptability.

Parameter	Symbol	Fitted value	Unit	Accepted range
Convection coefficient of air (bag side)	h_1	6	$W\ m^{-2}\ K^{-1}$	0.5–50 [62]
Convection coefficient of air (mold side)	h_2	0.5	$W\ m^{-2}\ K^{-1}$	
Initial initiator efficiency	f_0	0.5		0.3–0.8 [63]
Activation energy for initiator decomposition	E_d	63.25	$kJ\ mol^{-1}$	50–100 [64]
Normalised initiator diffusion coefficient	D_i^0/C	12.5		10^{-4}-10^4 [30,34]
Overlap factor monomer	γ_m	0.8		0–2 [28,30,34,65]
Overlap factor macroradical	γ_t	1.8		
Overlap factor initiator	γ_i	0.05		
Pre-exponential factor of PMMA diffusion coefficient	D_p	3×10^{-6}	$m^2\ s^{-1}$	10^{-7}–10^{-5} [28,30]

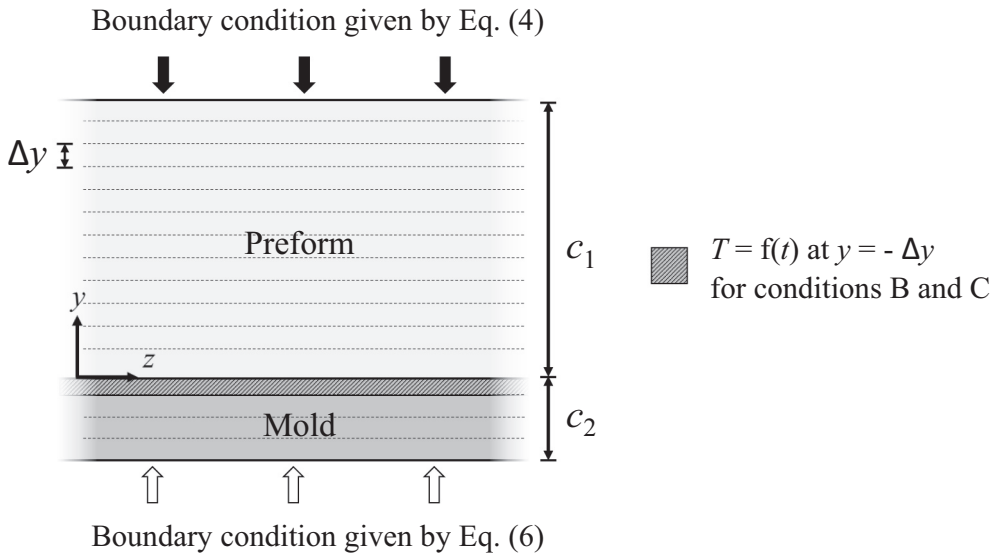

Fig. 4. Boundary conditions used in the 1D thermochemical model. Note that c_1 refers to preform thickness ($c_1 = 49$ mm for condition C and $c_1 = 73$ mm for conditions A and B) and c_2 is the thickness of the mold ($c_2 = 15$ mm). The time-dependent temperature profile applied at node $y = -\Delta y$ for testing conditions B and C is given in Fig. 2.

The contrast in void content between plates A and B can be related to the difference in the time-temperature profiles. The boiling temperature T_b of the MMA monomer is close to 101 °C at a pressure equal to 1 bar [58]. Note that the pressure inside the vacuum bag rises back to a value close to, but below, atmospheric pressure upon impregnation of the preform.[1] The value of T_b may therefore be lower than 101 °C (e.g. $T_b = 94$ °C at a pressure equal to 0.8 bar [3]), but in the remainder of this text we will assume $T_b = 101$ °C as a first-order approximation. The measured temperature T_t exceeds T_b at the mid-height and top of plate B, see Fig. 6a. This results in the observed void content in plate B at these locations. In contrast, the measured value of T_t remains below T_b throughout the polymerization of plate A, leading to a porosity close to zero across the thickness of the plate. In passing, we note that voids nucleated due to monomer boiling are unlikely to move due to buoyancy: the shear viscosity of infusion-grade MMA-based resins at the onset of the gel effect is close to 10 Pa·s, i.e. 100 times larger than the shear viscosity at the start of the polymerization [20,68]. The presence of the fiber tows is an additional obstacle to any movement across the thickness of the plate. Therefore, we expect the observed gradient in porosity in plate B to correspond to the observed increase in peak temperature across the thickness, see Fig. 6a. The difference in porosity between plates A and B demonstrates how external heating during vacuum infusion of an MMA-based resin may influence the microstructure of the polymerized composite part. Heating programs are typically used to shorten the manufacturing time. This is also illustrated in Fig. 6a: the end of the reaction (when the peak temperature, T_{max}, is reached) occurs three hours earlier in plate B compared to plate A which has an identical thickness.

We now explore the effect of preform thickness c_1 on the measured temperature profile. The measured temperature T_t in plates B ($c_1 = 73$ mm) and C ($c_1 = 49$ mm) at three locations across the thickness is plotted as a function of process time t in Fig. 6b. Note that both plates are subjected to the heating program summarized in Fig. 2. The peak temperature values in plate B are close to 10 °C higher than in plate C. This result illustrates how the peak temperature (and, therefore, the possibility of cavitation due to monomer boiling) depends upon preform thickness c_1.

[1] Grimsley et al. [66] and Moghaddam [67] conducted infusion tests with an epoxy resin on a glass fiber preform with dimensions similar to plates A, B and C in this study. They measured the resin pressure inside the bag throughout the curing process and found that the pressure ranged between 0.7 and 1 bar when the resin inlet and vacuum outlet were clamped shut after infusion.

4.2. Model calibration

The calibration parameters of the model presented in section 3 have been identified by using the measured temperature profiles of a single infusion and polymerization test (plate B). These fitting parameters are summarized in Table 4 and have been adjusted in order to match the predicted T_t versus t profiles with the measured ones for the three measurement locations across the thickness of plate B. Note that a physically acceptable range for each calibration parameter is defined in Table 4 and imposed to the fitted value of each parameter. The temperature profiles predicted by the calibrated model are included in Fig. 7: good agreement is observed between the model predictions and the measurements after identification, but this is not a sufficient validation of the model yet. We note in passing that, without the calibration step, the structural response of the predicted T versus t profiles is close to the measured ones. For instance, the model predicts the typical observed shape of the temperature-time response close to the peak in temperature. The thermochemical framework also predicts a dependence of peak time t_{peak} upon preform thickness and a sensitivity of peak width to the measurement location across the thickness of the preform.

The predicted values for the termination rate coefficient k_t, the propagation rate coefficient k_p and initiator efficiency f are plotted as a function of monomer conversion χ in Fig. 8, for a selected measurement location across the thickness of plate B. The curves obtained with the calibrated model are consistent with experimental data found in the literature for the bulk polymerization of methacrylic monomers [69,70]. The moderate increase of the value of k_p from $\chi = 0$ to $\chi = 0.8$ is due to the temperature increase in the preform. Four successive regimes are identified in Fig. 8, these correspond to the conversion regions defined by Achilias and co-workers [28–30]. The first regime corresponds to a free-radical polymerization mechanism in the absence of any

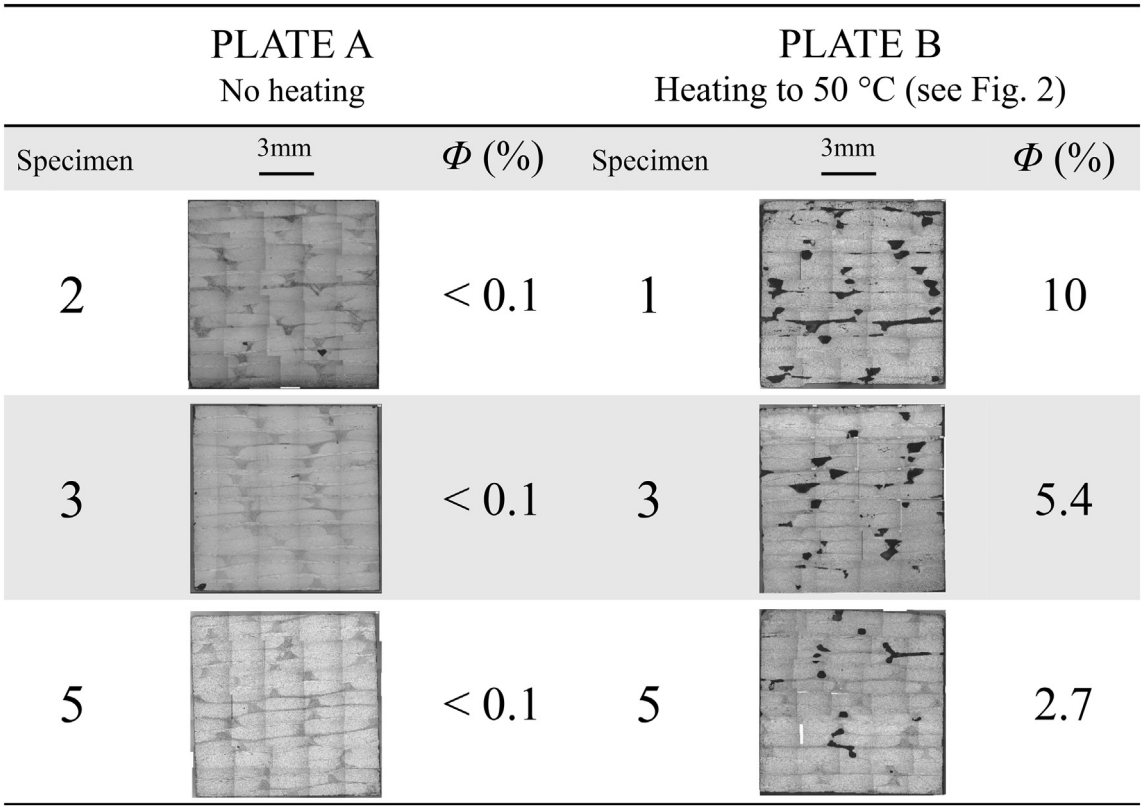

Fig. 5. Dependence of the measured porosity Φ upon measurement height for plates A and B (c_1= 73 mm). Note that measurement height is defined via the sectioning numbers given in Fig. 3.

diffusional limit. At the onset of the second regime, the value of k_t decreases with increasing χ due to the gel effect: the macroradicals lose translational mobility. When the reaction proceeds and χ further increases, the propagation-related radical mobility starts to dominate and the value of k_t plateaus. This plateau corresponds to regime 3. When χ continues to increase, both radical propagation and termination rates abruptly decrease, indicating the onset of regime 4. The initiator efficiency factor f also decreases with increasing monomer conversion in regime 4 due to the cage effect.

4.3. Model validation based on temperature profile predictions

The calibrated model is now validated based on the experimental temperature profiles measured for plates A and C. The predicted and measured T_t versus t response at three locations across the thickness of preforms A and C is plotted in Fig. 9a and b, respectively. Recall the differences in processing conditions for plates A, B and C: plate A is polymerized without an external heating program, while plate C is thinner (c_1= 49 mm) than plate B (c_1= 73 mm), see Table 1. There is an

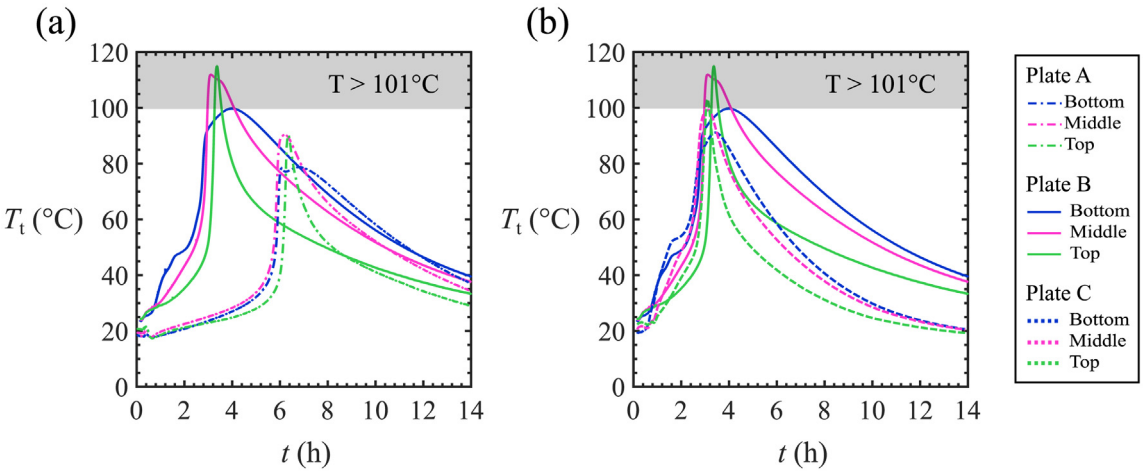

Fig. 6. Measured temperature T_t as a function of process time t at different locations across the thickness of (a) plates A and B and (b) plates B and C. See Table 1 for the y-coordinate corresponding to each measurement location.

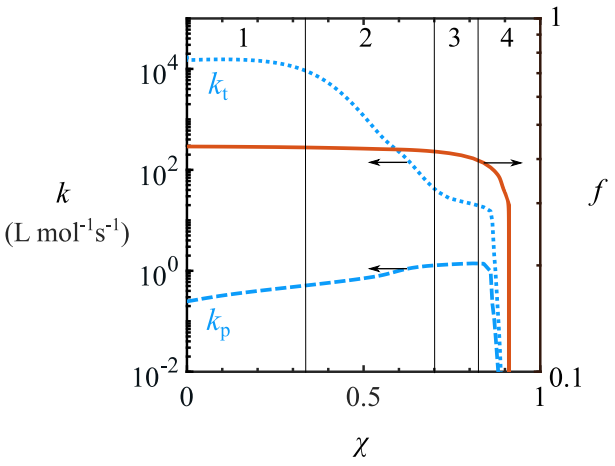

Fig. 8. Predicted values of k_p, k_t, and f as a function of monomer conversion χ by the calibrated model during the in-situ polymerization of the MMA-based resin at the bottom of plate B ($y \approx 0.06c_1$). Four conversion regimes are identified.

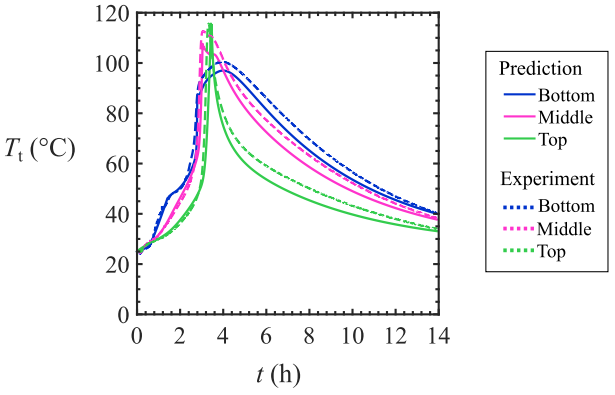

Fig. 7. Model identification by making use of the measured temperature profiles in plate B: measured (solid lines) and predicted (dashed lines) temperature T_t as a function of process time t at different locations across the thickness of the plate. See Table 1 for the y-coordinate corresponding to each measurement location.

excellent agreement between the predicted and measured temperature profiles for both testing conditions A and C. The peak temperature, peak time and the shape of the temperature profiles are accurately captured.

In addition, the predicted sensitivity of the T_t versus t response to the measurement position across the thickness of the preform is in line with the measurement data.

4.4. Conversion predictions

The predicted degree of monomer conversion χ is plotted as a function of process time t for tests A, B, and C in Fig. 10a, b and c, respectively. The shape of the χ versus t curves in Fig. 10 is close to identical for the three test conditions. First, the rate of monomer conversion is slow, and the slope of the χ versus t curve only moderately increases as the reaction proceeds. This corresponds to the first conversion regime identified in Fig. 8, during which there is no diffusional constraint on the reaction. Then, at a critical value of χ between 0.2 and 0.4, the reaction auto-accelerates. The gel effect results in a steep rise of the χ versus t curves, corresponding to regimes 2 and 3 shown in Fig. 8. Finally, a plateau value of χ close to 0.9 is reached, which marks the end of the reaction. This conversion plateau is consistent with the final drop in the values of k_p, k_t and f observed in regime 4, see Fig. 8. The predicted plateau value of χ_{max} ranges between 0.9 and 0.95 for the explored range of processing conditions, with a negligible dependence upon measurement location across the thickness. This value of χ_{max} is slightly lower than the measured values (between 0.95 and 0.99 [20,46,68]) for the resin under consideration when subjected to similar processing conditions. This small discrepancy can be attributed to the use of the QSSA (see section I.B of the Supplementary Information), and the assumption that the initial value of conversion χ is equal to zero. In practice, some chains are present in the resin before polymerization. These are added as a viscosifying agent but have an influence on the polymerization kinetics [3,21,34,71]. One may account for the presence of the PMMA chains by assuming a non-zero initial value for conversion [21]. However, it is unlikely that their rheological behavior is identical to that of a 'pure MMA system' at a non-zero conversion value. The treatment of this complex behavior is beyond the scope of the present study. We therefore follow Zoller [34], assume the initial value of χ to be zero, and realise that the predicted value of χ_{max} may be slightly below the typically measured value for χ_{max} as a consequence of this assumption.

The predicted conversion profiles shown in Fig. 10 demonstrate that the auto-acceleration of the reaction starts in the lower part of preforms A, B and C, and the time at which the gel effect takes place increases with increasing height. Recall from Fig. 7 (test B) and Fig. 9 (tests A and C) that the predicted and measured T_t versus t response at the top of the plates exhibits a sharper temperature rise and a higher peak temperature compared to the temperature profile at the bottom of the plate. This is attributed to the excess heat coming from the lower part

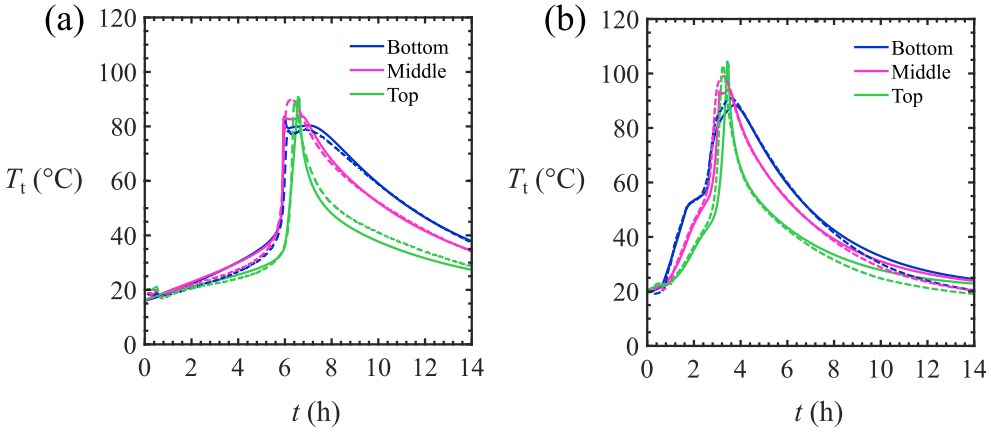

Fig. 9. Predicted (solid lines) and measured (dashed lines) temperature T_t as a function of process time t at different locations across the thickness of (a) plate A and (b) plate C. See Table 1 for the y-coordinate corresponding to each measurement location.

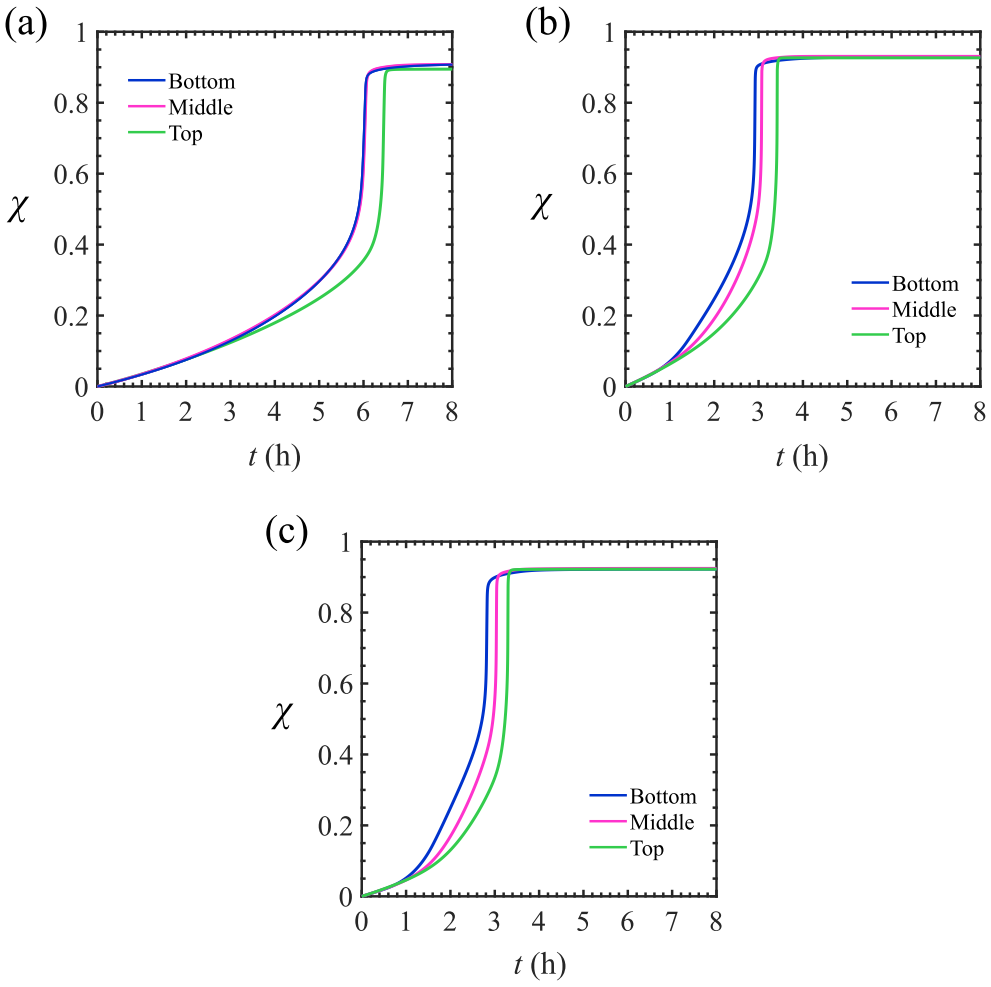

Fig. 10. Predicted degree of monomer conversion χ as a function of process time t for (a) plate A, (b) plate B and (c) plate C. See Table 1 for the y-coordinate corresponding to each measurement location.

of the plate, where the auto-acceleration of the reaction first takes place. This effect is more pronounced for the infusion of a thick plate with external heating, as shown in Fig. 7 via the temperature profiles for test B.

4.5. Processing maps

Optimal processing conditions for vacuum infusion with an MMA-based resin should lead to short polymerization times and laminates without thermally-induced voids. We assume that thermally-induced void nucleation (and growth) occurs when T_{max} at any location exceeds the boiling temperature of the monomer ($T_b = 101$ °C). We make use of the calibrated thermochemical model to illustrate how preform geometry, external heating conditions and the ambient temperature govern both T_{max} (and, therefore, the possibility of monomer boiling) and the (minimum) polymerization time. The simulations conducted for the predictions in this section are based on the values of the material and processing parameters given in Tables 3 and 4, unless stated otherwise.

The predicted value for T_{max} is plotted in Fig. 11a as a function of mold set temperature T_p for selected values of preform thickness c_1 and for a heating rate $\dot{q} = 0.5$ °C min^{-1} (and $T_{ext} = 25$ °C). The value of T_{max} increases with increasing T_p within the range 30 °C $< T_p <$ 70 °C for the explored range of preform thicknesses. In contrast, the value of T_{max} is almost insensitive to T_p for $T_p < 30$ °C and $T_p > 70$ °C. The predicted value of T_{max} is plotted in Fig. 11b as a function of mold heating rate $\dot{q}$ for selected values of preform thickness and for $T_p = 50$°C (and $T_{ext} = 25$ °C). The value of T_{max} is sensitive to $\dot{q}$ within the narrow range 0.12 °C min$^{-1} < \dot{q} <$ 0.5 °C min^{-1}. In addition, the predictions shown in Fig. 11a and b indicate that the processing window requiring $T_{max} < 101$ °C shrinks as the preform thickness increases. Note that the location for test B in Fig. 11a and b is included.

We proceed by exploring the sensitivity of the calculated peak temperature T_{max} to the ambient temperature T_{ext}. Fig. 11c shows the variation of T_{max} as a function of T_{ext} for three different preform thicknesses and in the absence of external heating (i.e. $\dot{q} = 0$). The value of T_{max} monotonously increases with increasing T_{ext}. The location of test A is included in Fig. 11c. The predictions shown in Fig. 11c also indicate that increasing the preform thickness leads to a reduction of the ambient temperature processing window: monomer boiling occurs when T_{ext} exceeds 35 °C for a preform thickness c_1 equal to 3 cm, while, for $c_1 =$ 7 cm, boiling already takes place when the infusion is conducted at an ambient temperature above 22 °C.

Structural and other functional requirements often dictate the thickness of the laminate. Wind turbine blades, for instance, comprise composite parts produced via vacuum infusion of thickness in the range 1 cm to 10 cm [3,72,73]. It is therefore convenient to construct a processing map with axes c_1 and T_p, and to plot the predicted boundary at which T_{max} is equal to 101 °C for selected values of heating rate, see Fig. 12a. For a given value of $\dot{q}$, the $T_{max} = 101$ °C boundary divides

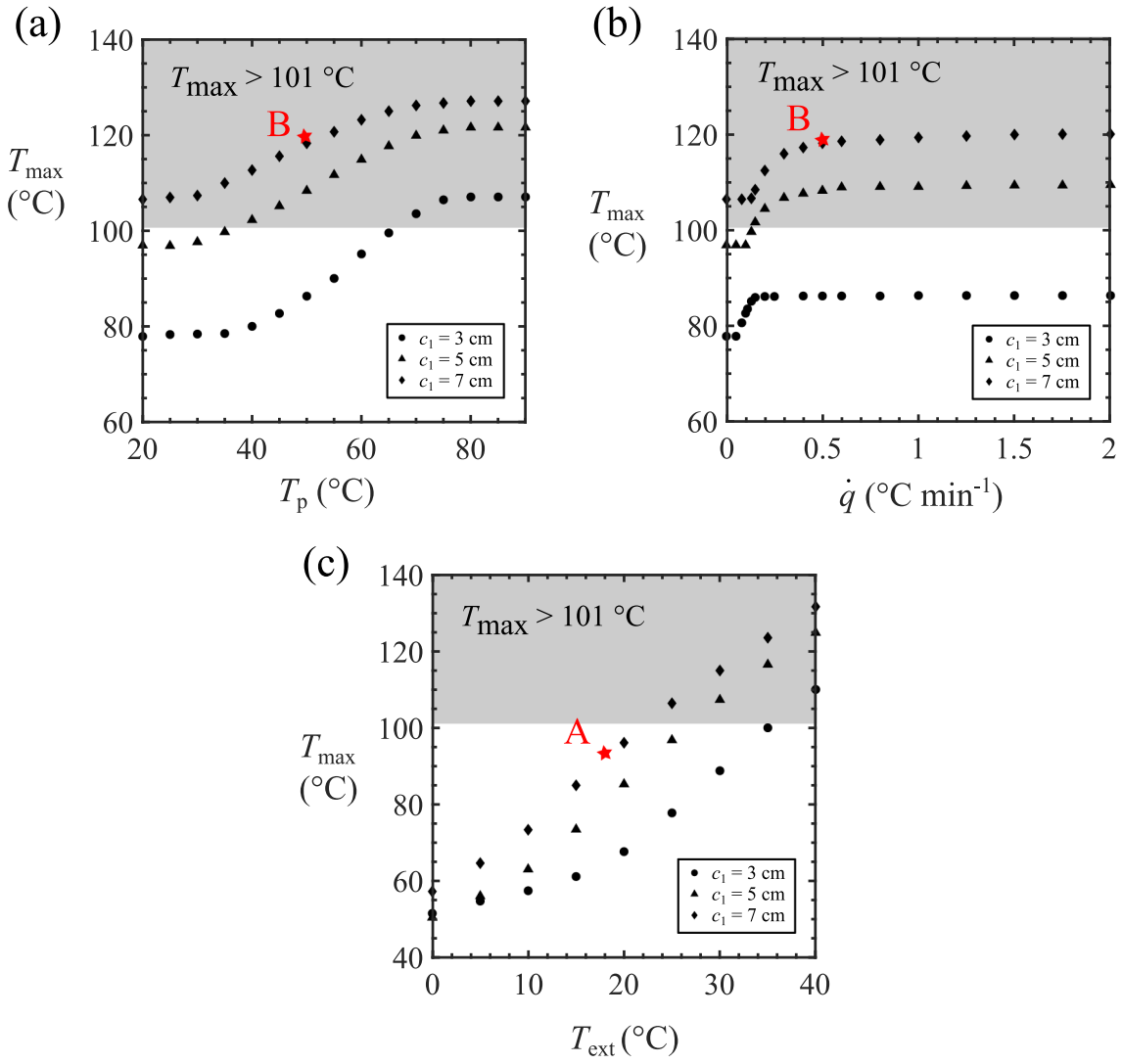

Fig. 11. Predicted maximum temperature in the preform during polymerization, T_{max}, as a function of (a) mold set temperature T_p for selected values of preform thickness c_1 ($\dot{q}$= 0.5 °C min^{-1} and T_{ext} = 25 °C) (b) heating rate $\dot{q}$ for selected values of c_1 (T_p = 50 °C, T_{ext} = 25 °C) and (c) ambient temperature T_{ext} for selected values of c_1 (for $\dot{q}$= 0). Manufacturing conditions corresponding to tests A and B are included.

the map into two regimes: a T_{max} < 101 °C window where no cavitation due to monomer boiling is expected, and a T_{max} ≥ 101 °C regime where monomer boiling is expected (this regime corresponds to the grey-shaded area in Fig. 12a for $\dot{q}$ = 0.2 °C min^{-1}). The T_{max} = 101 °C boundary is close to independent of the heating rate when the value of $\dot{q}$ is lower than 0.12 °C min^{-1} or exceeds 0.5 °C min^{-1}. The map shown in Fig. 12a is re-drawn in Fig. 12b for $\dot{q}$ = 1 °C min^{-1}. In addition, contours of equal values for the time at peak temperature t_{peak} for $\dot{q}$ = 1 °C min^{-1} are superimposed on the map. Recall that we assume the polymerization reaction ends at t close to t_{peak}. Three regimes are identified on the map shown in Fig. 12b. For a small preform thickness (c_1 < 2.3 cm), in regime I, the condition T_{max} = 101 °C can only occur when the mold set temperature is close to 101 °C. For an intermediate value of preform thickness (2.3 cm < c_1 < 5.6 cm), in regime II, the maximum mold set temperature T_p to prevent monomer boiling is a function of c_1. In addition, the optimum (minimum) process time t_{opt} for a thickness value of interest in regime II is obtained by finding the t_{peak} contour intersecting the T_{max} = 101 °C boundary at the selected value of preform thickness. For a large value of preform thickness (c_1> 5.6 cm), monomer boiling occurs irrespective of the selected value of $\dot{q}$ and T_p, and regime III is entered.

The three regimes (I, II and III) are plotted on a final processing map with axes c_1 and t_{opt}, see Fig. 13. Contours of equal values of the heating rate $\dot{q}$ in regimes I and II are included via the following method. The map shown in Fig. 12b is re-constructed for selected heating rates. For intermediate values of preform thickness (regime II), the value of t_{opt} is obtained as a function of c_1 by the intersection loci of the superimposed t_{peak} contours and the T_{max} = 101 °C boundary as explained above. For lower values of preform thickness, the slope of the T_{max} = 101 °C boundary becomes infinite, corresponding to the onset of regime I. In regime I, the value of t_{opt} corresponds to the peak time for a mold set temperature equal to 101 °C. The map shown in Fig. 13 yields the following useful insights. The minimum process time is almost independent of preform thickness in regime I. For low heating rates (i.e. $\dot{q}$ ≤ 0.1 °C min^{-1}) regime I encompasses the entire thickness range for which monomer boiling may be prevented

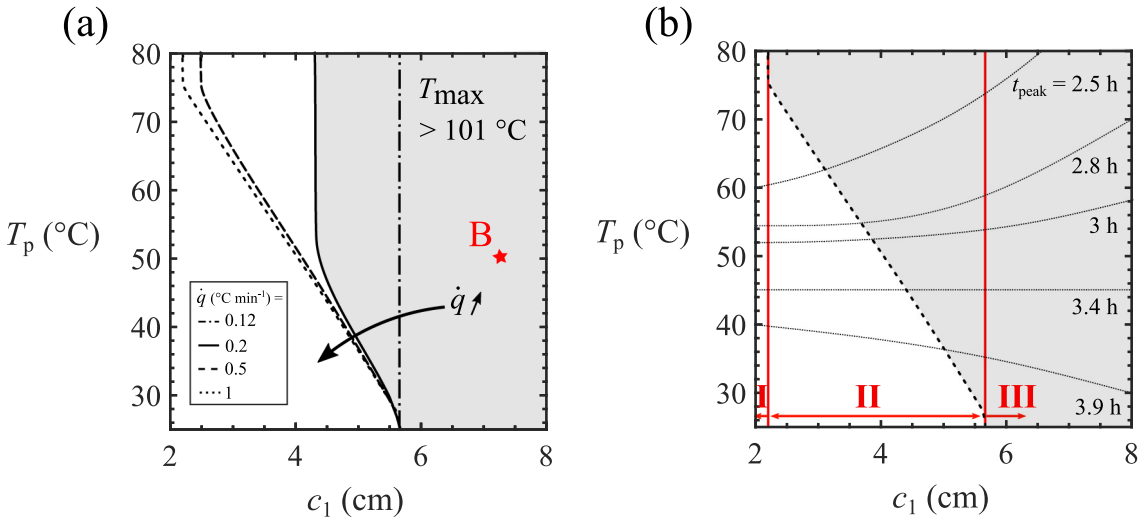

Fig. 12. Processing maps for the in-situ polymerization of an MMA-infused thick glass fiber preform: (a) mold set temperature T_p as a function of preform thickness c_1 with predicted $T_{max} = 101$ °C boundaries for selected values of heating rate ($T_{ext} = 25$ °C) and (b) mold set temperature T_p as a function of c_1 with predicted $T_{max} = 101$ °C boundary and contours of equal values of peak time t_{peak} for $\dot{q} = 1$ °C min^{-1} and $T_{ext} = 25$ °C.

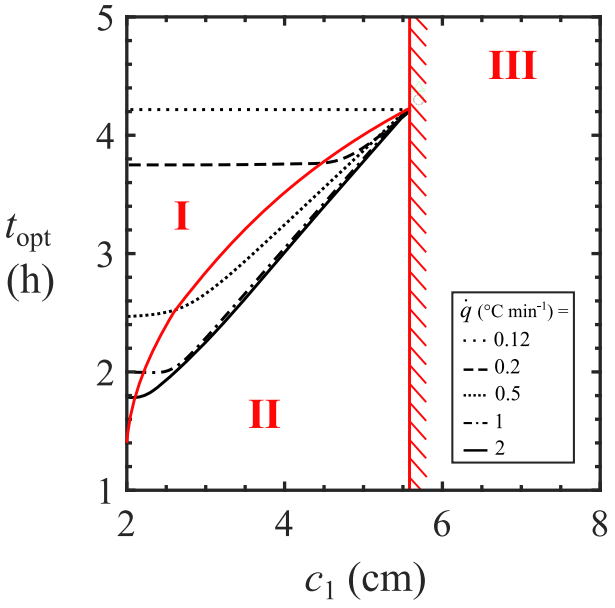

Fig. 13. Processing map of optimum (minimum) process time t_{opt} versus preform thickness c_1 for selected values of heating rate $\dot{q}$ ($T_{ext} = 25$ °C). The methods to determine the boundaries between regimes I, II and III are detailed in the text.

(i.e. $c_1 < 5.6$ cm). There is a strong dependence of t_{opt} upon the selected value of $\dot{q}$ in regime I. In contrast, the sensitivity of t_{opt} to $\dot{q}$ is low in regime II. For $\dot{q}$ exceeding 1 °C min^{-1} in regime II, the value of t_{opt} is a linear function of the preform thickness and is insensitive to $\dot{q}$ (i.e. increasing $\dot{q}$ does not result in a shorter process time). In addition, for the MMA-based resin of interest, the regime II to regime III boundary at c_1 close to 5.6 cm is found to be independent of the selected heating conditions.

5. Concluding remarks

A thermochemical model is developed to predict the temperature field across the thickness of a composite laminate processed by infusion and in-situ polymerization of a methyl methacrylate (MMA)-based resin. The main challenge is to limit void formation due to local monomer boiling which is the result of the auto-accelerating, exothermic polymerization reaction. The main findings of the present study are the following:

- The quasi-steady state approximation (QSSA) can be used to describe the self-accelerating polymerization reaction of MMA in a finite difference thermochemical model. The QSSA significantly reduces the computing cost of the model, yet it leads to accurate temperature and monomer conversion predictions up to a critical monomer conversion value close to 0.9.
- The occurrence of cavitation due to monomer boiling is highly sensitive to the selected mold heating program and to the thickness of the preform.
- The computationally efficient thermochemical model enables the construction of comprehensive processing maps, which can be used to reveal optimum mold heating conditions for the fast production of thick MMA-based preforms of a given thickness range without thermally-induced voids. There is, however, an upper bound on the preform thickness above which monomer boiling takes place irrespective of the selected heating program.

Data availability

The measurement data and code will be uploaded on the Open Data repository of UCLouvain: https://dataverse.uclouvain.be/.

Declaration of Competing Interest

The authors declare that they have no known competing financial interests or personal relationships that could have appeared to influence the work reported in this paper.

Acknowledgements

Financial support from Arkema is gratefully acknowledged. The authors would like to thank the Elium team at the Groupement de Recherche de Lacq (Lacq, France) for the assistance with the infusion

tests and Dr. J. Soete (KU Leuven) for the assistance with the micro-computed tomography measurements.

Appendix A. Supplementary data

Supplementary data to this article can be found online at https://doi.org/10.1016/j.matdes.2020.109170.

References

[1] J.J. Murray, C. Robert, K. Gleich, E.D. McCarthy, Ó Brádaigh CM., Manufacturing of unidirectional stitched glass fabric reinforced polyamide 6 by thermoplastic resin transfer moulding, Mater. Des. 189 (2020) https://doi.org/10.1016/j.matdes.2020.108512.

[2] D.S. Cousins, Y. Suzuki, R.E. Murray, J.R. Samaniuk, A.P. Stebner, Recycling glass fiber thermoplastic composites from wind turbine blades, J. Clean. Prod. 209 (2019) 1252–1263, https://doi.org/10.1016/j.jclepro.2018.10.286.

[3] D.S. Cousins, Advanced Thermoplastic Composites for Wind Turbine Blade Manufacturing, Colorado School of Mines, 2018.

[4] D. Mamalis, W. Obande, V. Koutsos, J.R. Blackford, Ó Brádaigh CM, Ray D., Novel thermoplastic fibre-metal laminates manufactured by vacuum resin infusion: the effect of surface treatments on interfacial bonding, Mater. Des. 162 (2019) 331–344, https://doi.org/10.1016/j.matdes.2018.11.048.

[5] S.K. Bhudolia, P. Perrotey, S.C. Joshi, Optimizing polymer infusion process for thin ply textile composites with novel matrix system, Materials 10 (2017) 293, https://doi.org/10.3390/ma10030293.

[6] M.E. Kazemi, L. Shanmugam, D. Lu, X. Wang, B. Wang, J. Yang, Mechanical properties and failure modes of hybrid fiber reinforced polymer composites with a novel liquid thermoplastic resin, Elium®, Compos. A: Appl. Sci. Manuf. 125 (2019) https://doi.org/10.1016/j.compositesa.2019.105523.

[7] N.C.W. Judd, W.W. Wright, Voids and their effects on the mechanical properties of composites - an appraisal, SAMPE J. 14 (1978) 10–15.

[8] L. Maragoni, P.A. Carraro, M. Peron, M. Quaresimin, Fatigue behaviour of glass/epoxy laminates in the presence of voids, Int. J. Fatigue 95 (2017) 18–28, https://doi.org/10.1016/j.ijfatigue.2016.10.004.

[9] T. Hayashi, J. Takahashi, Influence of void content on the flexural fracture behaviour of carbon fiber reinforced polypropylene, J. Compos. Mater. 51 (2017) 4067–4078, https://doi.org/10.1177/0021998317698215.

[10] F. Van Loock, M.D. Thouless, N.A. Fleck, Tensile fracture of an adhesive joint: the role of crack length and of material mismatch, J. Mech. Phys. Solids. 130 (2019) 330–348, https://doi.org/10.1016/j.jmps.2019.06.004.

[11] M. Mehdikhani, N.A. Petrov, I. Straumit, A.R. Melro, S.V. Lomov, L. Gorbatikh, The effect of voids on matrix cracking in composite laminates as revealed by combined computations at the micro- and meso-scales, Compos. Part A Appl. Sci. Manuf. 117 (2019) 180–192, https://doi.org/10.1016/j.compositesa.2018.11.009.

[12] J.L. Kardos, R. Dave, N.P. Dudukovic, Voids in composites, in: T.G. Gutowski (Ed.), The manufacturing Science of Composites, Proceedings of Manufacturing International ' 88, vol. 4, Atlanta, Georgia (USA) 1988, pp. 41–48.

[13] T.S. Lundstrom, B.R. Gebart, C.Y. Lundemo, Void formation in RTM, J. Reinf. Plast. Compos. 12 (1993) 1339–1349, https://doi.org/10.1177/073168449301201207.

[14] N. Patel, V. Rohatgi, L.J. Lee, Micro scale flow behavior and void formation mechanism during impregnation through a unidirectional stitched fiberglass mat, Polym. Eng. Sci. 35 (1995) 837–851, https://doi.org/10.1002/pen.760351006.

[15] M. Afendi, W. Banks, D. Kirkwood, Bubble free resin for infusion process, Compos. Part A Appl. Sci. Manuf. 36 (2005) 739–746, https://doi.org/10.1016/j.compositesa.2004.10.030.

[16] M. Mehdikhani, L. Gorbatikh, I. Verpoest, S.V. Lomov, Voids in fiber-reinforced polymer composites: a review on their formation, characteristics, and effects on mechanical performance, J. Compos. Mater. 53 (2019) 1579–1669, https://doi.org/10.1177/0021998318772152.

[17] N. Patel, L.J. Lee, Modeling of void formation and removal in liquid composite molding. Part II: model development and implementation, Polym. Compos. 17 (1996) 104–114, https://doi.org/10.1002/pc.10595.

[18] L. Labat, J. Bréard, S. Pillut-Lesavre, G. Bouquet, Void fraction prevision in LCM parts, Eur. Phys. J. Appl. Phys. 16 (2001) 157–164, https://doi.org/10.1051/epjap:2001104.

[19] J. Bréard, Y. Henzel, F. Trochu, R. Gauvin, Analysis of dynamic flows through porous media. Part I: comparison between saturated and unsaturated flows in fibrous reinforcements: analysis of dynamic flows. I, Polym. Compos. 24 (2003) 391–408.

[20] Q. Charlier, Adhesion Phenomena in Thermoplastic Composites Based on Acrylic Matrices Obtained by Free Radical Polymerization, Institut National des Sciences Appliquées de Lyon, 2015.

[21] Y. Suzuki, D.S. Cousins, J. Wassgren, B.B. Kappes, J. Dorgan, A.P. Stebner, Kinetics and temperature evolution during the bulk polymerization of methyl methacrylate for vacuum-assisted resin transfer molding, Compos. Part A Appl. Sci. Manuf. 104 (2018) 60–67, https://doi.org/10.1016/j.compositesa.2017.10.022.

[22] V.E. Trommsdorff, H. Köhle, P. Lagally, Zur polymerisation des methacrylsäuremethylesters, Die Makromolekulare Chemie 1 (1948) 169–198, https://doi.org/10.1002/macp.1948.020010301.

[23] W. Obande, D. Mamalis, D. Ray, L Yang .O., C.M. Brádaigh, Mechanical and thermomechanical characterisation of vacuum-infused thermoplastic- and thermoset-based composites, Mater. Des. (2019) 175, https://doi.org/10.1016/j.matdes.2019.107828.

[24] R.G.W. Norrish, R.R. Smith, Catalyzed polymerization of methyl methacrylate in the liquid phase, Nature 150 (1942) 336–337, https://doi.org/10.1038/150336a0.

[25] F.L. Marten, A.E. Hamielec, High conversion diffusion-controlled polymerization, in: J.N. Henderson (Ed.), Polymerization Reactors and Processes, ACS Symposium Series, vol. 104, American Chemical Society, Washington, DC (USA) 1979, pp. 43–70, https://doi.org/10.1021/bk-1979-0104.ch003.

[26] A.E. Hamielec, Recent developments in free-radical polymerization at high conversion - diffusion-controlled termination and propagation, Chem. Eng. Commun. 24 (1983) 1–19, https://doi.org/10.1080/00986448308940070.

[27] S. Zhu, A.E. Hamielec, Chain-length-dependent termination for free radical polymerization, Macromolecules 22 (1989) 3093–3098, https://doi.org/10.1021/ma00197a033.

[28] D. Achilias, C. Kiparissides, Modeling of diffusion-controlled free-radical polymerization reactions, J. Appl. Polym. Sci. 35 (1988) 1303–1323, https://doi.org/10.1002/app.1988.070350516.

[29] D.S. Achilias, C. Kiparissides, Development of a general mathematical framework for modeling diffusion-controlled free-radical polymerization reactions, Macromolecules 25 (1992) 3739–3750, https://doi.org/10.1021/ma00040a021.

[30] D.S. Achilias, I.D. Sideridou, Kinetics of the benzoyl peroxide/amine initiated free-radical polymerization of dental Dimethacrylate monomers: experimental studies and mathematical modeling for TEGDMA and Bis-EMA, Macromolecules 37 (2004) 4254–4265, https://doi.org/10.1021/ma049803n.

[31] A.W. Hui, A.E. Hamielec, Thermal polymerization of styrene at high conversions and temperatures. An experimental study, J. Appl. Polym. Sci. 16 (1972) 749–769, https://doi.org/10.1002/app.1972.070160319.

[32] N. Tefera, G. Weickert, K.R. Westerterp, Modeling of free radical polymerization up to high conversion. II. Development of a mathematical model, J. Appl. Polym. Sci. 63 (1997) 1663–1680, https://doi.org/10.1002/(SICI)1097-4628(19970321)63:12%3C1663::AID-APP17%3E3.0.CO;2-0.

[33] J.S. Sangwai, S.A. Bhat, S. Gupta, D.N. Saraf, S.K. Gupta, Bulk free radical polymerizations of methyl methacrylate under non-isothermal conditions and with intermediate addition of initiator: experiments and modeling, Polymer 46 (2005) 11451–11462, https://doi.org/10.1016/j.polymer.2005.10.064.

[34] A. Zoller, D. Gigmes, Y. Guillaneuf, Simulation of radical polymerization of methyl methacrylate at room temperature using a tertiary amine/BPO initiating system, Polym. Chem. 6 (2015) 5719–5727, https://doi.org/10.1039/C5PY00229J.

[35] A.C. Loos, G.S. Springer, Curing of epoxy matrix composites, J. Compos. Mater. 17 (1983) 135–169, https://doi.org/10.1177/002199838301700204.

[36] T.A. Bogetti, J.W. Gillespie, Two-dimensional cure simulation of thick thermosetting composites, J. Compos. Mater. 25 (1991) 239–273, https://doi.org/10.1177/002199839102500302.

[37] T.E. Twardowski, S.E. Lin, P.H. Geil, Curing in thick composite laminates: experiment and simulation, J. Compos. Mater. 27 (1993) 216–250 doi:0.1177/002199839302700301.

[38] M.K. Telikicherla, M.C. Altan, F.C. Lai, Autoclave curing of thermosetting composites: process modeling for the cure assembly, Int. Commun. Heat Mass. 21 (1994) 13, https://doi.org/10.1016/0735-1933(94)90032-9.

[39] D.C. Blest, B.R. Duffy, S. McKee, A.K. Zulkifle, Curing simulation of thermoset composites, Compos. Part A Appl. Sci. Manuf. 30 (1999) 1289–1309, https://doi.org/10.1016/S1359-835X(99)00032-9.

[40] E. Ruiz, F. Trochu, Numerical analysis of cure temperature and internal stresses in thin and thick RTM parts, Compos. Part A Appl. Sci. Manuf. 36 (2005) 806–826, https://doi.org/10.1016/j.compositesa.2004.10.021.

[41] S. Anandan, G.S. Dhaliwal, Z. Huo, K. Chandrashekhara, N. Apetre, N. Iyyer, Curing of thick thermoset composite laminates: multiphysics modeling and experiments, Appl. Compos. Mater. 25 (2018) 1155–1168, https://doi.org/10.1007/s10443-017-9658-9.

[42] M. Ren, Q. Wang, J. Cong, X. Chang, Study of one-dimensional cure simulation applicable conditions for thick laminates and its comparison with three-dimensional simulation, Sci. Eng. Compos. Mater. 25 (2018) 1197–1204, https://doi.org/10.1515/secm-2017-0244.

[43] A. Borzacchiello, L. Ambrosio, L. Nicolais, E.J. Harper, K.E. Tanner, W. Bonfield, Isothermal and non-isothermal polymerization of a new bone cement, J. Mater. Sci. Mater. Med. 9 (1998) 317–324, https://doi.org/10.1023/A:1008898712929.

[44] J.J.E. Teuwen, A.A. van Geenen, H.E.N. Bersee, Temperature evolution during processing of thick-walled anionic polyamide 6 composites: experiment and simulation, Macromol. Mater. Eng. 298 (2013) 722–729, https://doi.org/10.1002/mame.201200083.

[45] C.A. Schneider, W.S. Rasband, K.W. Eliceiri, NIH image to ImageJ: 25 years of image analysis, Nat. Methods 9 (2012) 671–675, https://doi.org/10.1038/nmeth.2089.

[46] S.G. Gayot, C. Bailly, T. Pardoen, P. Gérard, Relationship between processing parameters and mechanical properties of thick glass fibre reinforced thermoplastic methacrylic composites, in: A. Turon, P. Maimí, M. Fagerström (Eds.),Proceedings of the 7th ECCOMAS Thematic Conference on the Mechanical Response of Composites, Girona, Spain, 2019.

[47] N.A. Dotson, R. Galvan, R.L. Laurence, M. Tirrell, Polymerization Process Modeling, VCH Publishers, Inc., New York, NY (USA), 1996.

[48] H. Fujita, Diffusion in polymer-diluent systems, Fortschr. Hochpolym. Forsch. 3 (1961) 1–47, https://doi.org/10.1007/BFb0050514.

[49] J.S. Vrentas, J.L. Duda, Diffusion in polymer—solvent systems. I. Reexamination of the free-volume theory, J. Polym. Sci. Polym. Phys. 15 (1977) 403–416, https://doi.org/10.1002/pol.1977.180150302.

[50] M.F. Ashby, Materials Selection in Mechanical Design, 4th ed. Butterworth-Heinemann, Oxford (England), 2010.

[51] R. Greiner, F.R. Schwarzl, Thermal contraction and volume relaxation of amorphous polymers, Rheol. Acta 23 (1984) 378–395, https://doi.org/10.1007/BF01329190.

[52] J.E. Mark (Ed.), Physical Properties of Polymers Handbook, 2nd ed.Springer, New York, NY (USA), 2006.
[53] M. Karabaev, A.A. Saidov, T.P. Abduzhaminov, M.M. Kenisarin, Heat capacity and molecular kinetic processes of condensed phase acrylates and methacrylates, Izv Akad Nauk UzSSR, Ser Fiz-Mat Nauk 6 (1985) 51–54.
[54] J. Brandrup, E.H. Immergut, E.A. Grulke (Eds.), Polymer Handbook, 4th ed.Wiley, New York, NY (USA), 1999.
[55] M. Bauccio, ASM Engineered Materials Reference Book, 2nd ed. Ed. ASM International, Materials Park, OH (USA), 1994.
[56] J.N. Cardenas, K.F. O'Driscoll, High-conversion polymerization. I. Theory and application to methyl methacrylate, J. Polym. Sci. A Polym. Chem. 14 (1976) 883–897, https://doi.org/10.1002/pol.1976.170140409.
[57] G.T. Russell, D.H. Napper, R.G. Gilbert, Termination in free-radical polymerizing systems at high conversion, Macromolecules 21 (1988) 2133–2140, https://doi.org/10.1021/ma00185a044.
[58] W.M. Haynes, CRC Handbook of Chemistry and Physics, 97th ed. CRC Press, Taylor & Francis Group, Boca Raton, FL (USA), 2017.
[59] S. Beuermann, M. Buback, T.P. Davis, R.G. Gilbert, R.A. Hutchinson, Olaj OF, et al., Critically evaluated rate coefficients for free-radical polymerization, 2.†. Propagation rate coefficients for methyl methacrylate, Macromol. Chem. Phys. 198 (1997) 1545–1560, https://doi.org/10.1002/macp.1997.021980518.
[60] D.R. Taylor, K.Y. van Berkel, M.M. Alghamdi, G.T. Russell, Termination rate coefficients for radical Homopolymerization of methyl methacrylate and styrene at low conversion, Macromol. Chem. Phys. 211 (2010) 563–579, https://doi.org/10.1002/macp.200900668.
[61] S.S. Meadows, M.V. Hosur, A. Tcherbi-Narteh, S. Jeelani, Kinetic analysis of different peroxide initiators on the cure behavior of bio-based and recycled unsaturated polyester Envirez resins, CAMX Conference Proceedings, Dallas, TX (USA) 2015, p. 14.
[62] J.H. Lienhard, J.H. Lienhard, A Heat Transfer Textbook, 5th ed. Phlogiston Press, Cambridge, MA (USA), 2019.
[63] G.G. Odian, Principles of Polymerization, 4th ed. Wiley-Interscience, Hoboken, NJ (USA), 2004.
[64] E.T. Denisov, T.G. Denisova, T.S. Pokidova, Handbook of Free Radical Initiators, 1st ed. Wiley-Interscience, Hoboken, NJ (USA), 2003.
[65] D.L. Kurdikar, N.A. Peppas, A kinetic model for diffusion-controlled bulk crosslinking Photopolymerizations, Macromolecules 27 (1994) 4084–4092, https://doi.org/10.1021/ma00093a009.
[66] B.W. Grimsley, P. Hubert, X. Song, R.J. Cano, A.C. Loos, R.B. Pipes, Flow and Compaction During the Vacuum Assisted Resin Transfer Molding Process, Proceedings of 33rd ISTC, Seattle, WA (USA), 2001 1–14.
[67] M. Moghaddam, A. Breede, C. Brauner, W. Lang, Embedding Piezoresistive pressure sensors to obtain online pressure profiles inside Fiber composite laminates, Sensors 15 (2015) 7499–7511, https://doi.org/10.3390/s150407499.
[68] J.-C. Fontanier, Développement d'un système réactif pour composites acryliques par procédé RTM, Institut National des Sciences Appliquées de Lyon, 2017.
[69] P. Hayden, H. Melville, The kinetics of the polymerization of methyl methacrylate. I. the bulk reaction, J. Polym. Sci. 43 (1960) 201–214, https://doi.org/10.1002/pol.1960.1204314116.
[70] S. Zhu, Y. Tian, A.E. Hamielec, D.R. Eaton, Radical concentrations in free radical copolymerization of MMA/EGDMA, Polymer 31 (1990) 154–159, https://doi.org/10.1016/0032-3861(90)90368-9.
[71] A.G. Gibson, J.-A. Månson, Impregnation technology for thermoplastic matrix composites, Compos. Manuf. 3 (1992) 223–233, https://doi.org/10.1016/0956-7143(92)90110-G.
[72] P.P. Parlevliet, Residual Strains in Thick Thermoplastic Composites an Experimental Approach, Technische Universiteit Delft, 2010.
[73] P. Brøndsted, H. Lilholt, A. Lystrup, Composite materials for wind power turbine blades, Annu. Rev. Mater. Res. 35 (2005) 505–538, https://doi.org/10.1146/annurev.matsci.35.100303.110641.